LA-UR-01-1424

Los Alamos National Laboratory is operated by the University of California for the United States Department of Energy under contract W-7405-ENG-36.

TITLE: # Sky View Factor Measurements in Downtown Salt Lake City - Data Report for the DOE CBNP URBAN Experiment, Oct. 2000

AUTHOR(S): Michael J. Brown, Los Alamos National Laboratory, Group D-4
Sue Grimmond, Indiana University, Geography Dept.

SUBMITTED TO: Internal Report
March, 2001

Los Alamos

Los Alamos National Laboratory
Los Alamos, New Mexico 87545

FORM NO. 836 R4
ST. NO. 2629 5/81

Sky View Factor Measurements in Downtown Salt Lake City - Data Report for the DOE CBNP URBAN Experiment, October 2000

Michael Brown[1] and Sue Grimmond[2]

[1]Los Alamos National Laboratory, Energy and Environmental Analysis Group D-4, MS F604, Los Alamos, NM 87545, mbrown@lanl.gov

[2]Indiana University, Atmospheric Science Program, Geography Dept., Student Building 104, 701 E. Kirkwood Ave, Bloomington. IN 47405-7100, grimmon@indiana.edu

Synopsis. As part of the October 2000 URBAN Field Experiment in Salt Lake City, upward pointing fish-eye photographs were taken in the downtown area from ground level in order to compute the sky view factor (Ψ_{sky}). Using image analysis and in-house processing software (Grimmond et al., 2001), Ψ_{sky} was computed for each photograph. In this report, we give a brief overview of what the sky view factor is, why it's important in meteorological studies of urban areas, and how it is computed from fish-eye photographs. The fish-eye images and the computed Ψ_{sky} are presented in both tables and maps. The range of Ψ_{sky} observed in Salt Lake City was from 0.33 to 0.90, with an average of 0.70 based on 93 images taken in the downtown area.

Introduction.

The ratio of the radiation received (or emitted) by a planar surface to the radiation emitted (or received) by the entire hemispheric environment is called the sky view factor Ψ_{sky} (Watson and Johnson, 1987). Sky view factor is used in radiation balance schemes to partition long and short-wave radiation within urban and forest canopies and complex terrain. In the urban environment, Ψ_{sky} and $1-\Psi_{sky}$ give a measure of how much radiation will penetrate the canopy and how much will be intercepted by the canopy, respectively. Ψ_{sky} is determined for a specific point in space, i.e., it gives a measure of the openness of the sky to radiative transport relative to a specific location. Ψ_{sky} varies from zero to one, where $\Psi_{sky} = 0$ means that the sky is completely obstructed by obstacles and all outgoing radiation would be intercepted by the obstacles (such a situation would occur in a tunnel, for example), while $\Psi_{sky} = 1$ means that there are no obstructions and all outgoing radiation would radiate freely to the sky. In the example shown in Fig. 1, the surrounding buildings cover 50% of the area of the sky. However, the sky view factor for this case is greater than 50% because it is weighted by the spread of the radiation over the surface of interest. For a flat surface at the ground, the incoming radiation from directly overhead spreads out over a smaller area, while radiation coming from near the horizon would spread out over a very large area, making the effective flux of radiation (W m^{-2}) small (Fig. 1b). Often Ψ_{sky} is analytically derived from subtracting off the view factors of the obstacles surrounding the point of interest, i.e., sky view factor equals one minus the sum of view factors between the surface of interest (for example, a street) and the surrounding obstacles in the field of view (for example, building walls).

This data report provides information on sky view factor measurements taken in Salt Lake City as part of the DOE CBNP URBAN field experiment conducted in October 2000. Before presenting results, we provide background material on the sky view factor. In the next section we give an

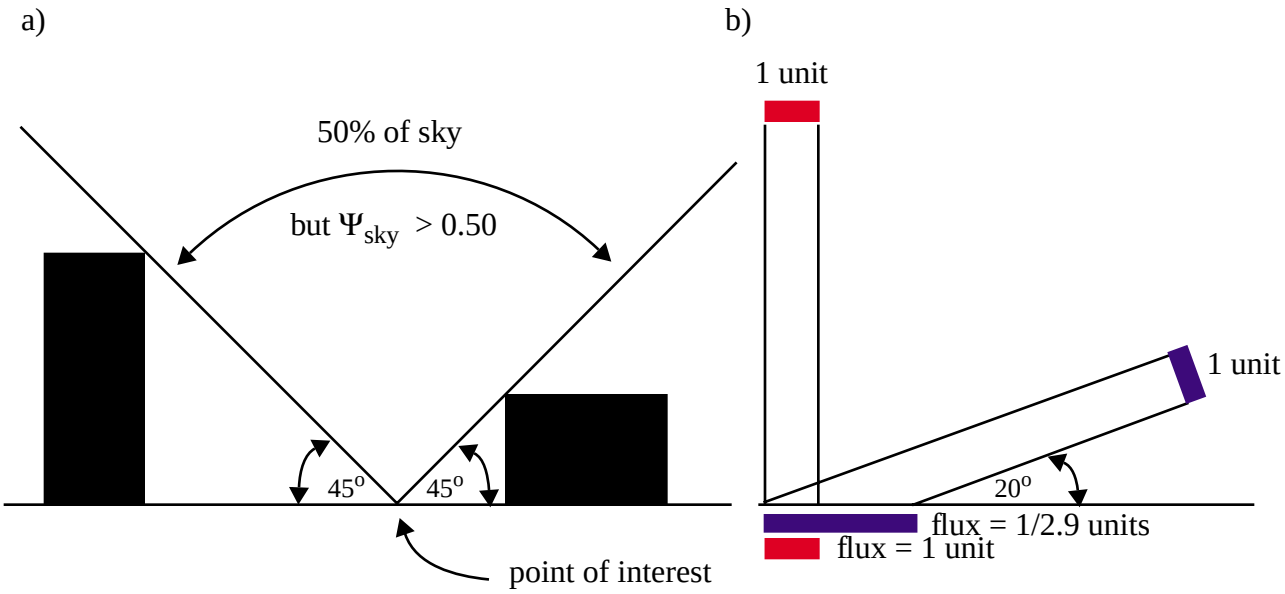

Figure 1. a) A 2-D example showing that 50% of the view is open to the sky relative to the point of interest at the surface, but as shown in b) the sky view factor for this case is greater than 0.5 because it weights the open area by the radiation intensity.

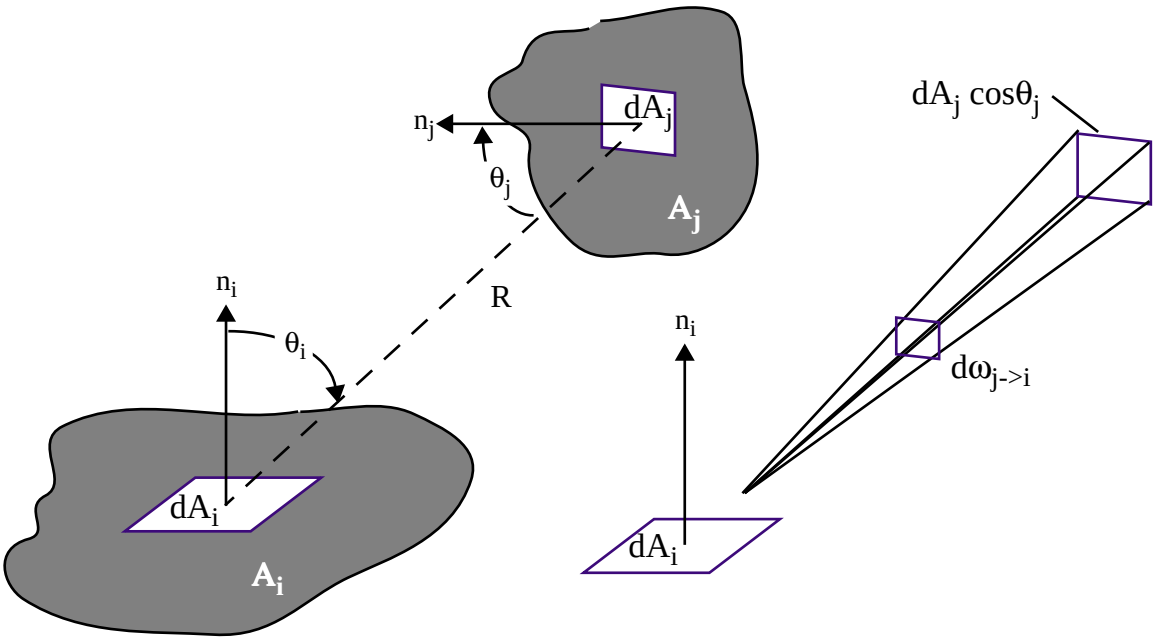

Figure 2. Variables used in the calculation of the view factor between two elemental surfaces dA_i and dA_j (from Incropera and DeWitt, 1996).

overview of the derivation of view factors between surfaces. We then follow with brief sections on sky view factor applications in urban meteorology and the methodology for computing Ψ_{sky} from fish-eye images. We conclude by showing the computed sky view values for downtown Salt Lake City in table and map format, and a listing of the availability and organization of this dataset on the URBAN web server.

View Factor Derivation.

The view factor is used when computing radiation exchanges between two surfaces. It is defined as the fraction of the radiation leaving surface A_i that is intercepted by surface A_j (Incropera and DeWitt, 1996):

$$\Psi_{ij} = \frac{q_{i \to j}}{A_i J_i}, \tag{1}$$

where $q_{i \to j}$ [W] is the total radiation emitted from A_i intercepted by surface A_j, and J_i [W m^{-2}] is the radiosity of surface A_i, such that $A_i J_i$ is the total amount of radiation emitted from surface A_i. The view factor is a dimensionless quantity that varies from 0 to 1, where $\Psi_{ij} = 0$ indicates that none of the radiation emitted from surface A_i is intercepted by surface A_j, while $\Psi_{ij} = 1$ signifies that all of the radiation was intercepted. The radiation exchange from one surface to another is highly dependent on the shape, surface geometry, and relative orientations of the two surfaces. Given the two arbitrary surfaces A_i and A_j with sub-areas dA_i and dA_j separated by a distance R (see Fig. 2), the radiation leaving dA_i and intercepting dA_j can be expressed as:

$$dq_{i \to j} = I_i \cos\theta_i dA_i d\omega_{j \to i} \,, \tag{2}$$

where I_i [W sr^{-1}] is the radiation intensity leaving surface A_i, θ_i is the polar angle between the normal vector n_i and line R, and $d\omega_{j->i}$ is the solid angle subtended by dA_j as viewed from dA_i. Given that $d\omega_{j->i} = (\cos\theta_j \, dA_j)/R^2$ and assuming that surface A_i emits and reflects diffusely and isotropically (i.e., uniformly in all directions) such that $I_i = J_i/\pi$, one can integrate over the two surfaces to obtain the total radiation leaving A_i and intercepted by A_j:

$$q_{i \to j} = J_i \int_{A_i} \int_{A_j} \frac{\cos\theta_i \cos\theta_j}{\pi R^2} dA_i dA_j \,, \tag{3}$$

where the radiosity J_i has been pulled out of the integral by assuming that it is constant over the surface A_i. Substituting into eqn. (1), we obtain:

$$\Psi_{ij} = \frac{1}{A_i} \int_{A_i} \int_{A_j} \frac{\cos\theta_i \cos\theta_j}{\pi R^2} dA_i dA_j \,. \tag{4}$$

The view factor Ψ_{ji} is identical to eqn. (4), except that $1/A_i$ is replaced by $1/A_j$. Hence $A_i\Psi_{ij} = A_j\Psi_{ji}$.

Summation over all obstacle surfaces would give a terrain or canopy view factor for surface A_i:

$$\Psi_{canopy} = \sum_{j=1}^{\text{all sfcs. } A_j} \Psi_{ij} \,. \tag{5}$$

The sky view factor is then just

$$\Psi_{sky} = 1 - \Psi_{canopy} \,. \tag{6}$$

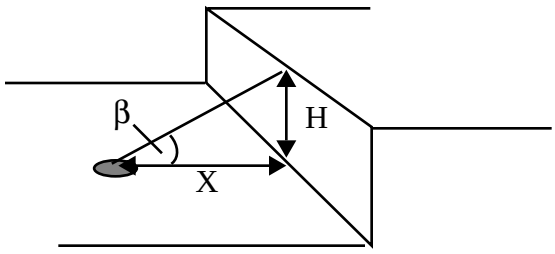

Figure 3. Geometric configuration for the sky and canopy view factor solutions given in eqns. (7a) and (7b) (from Oke, 1987).

Numerous analytical solutions can be derived for idealized geometries (e.g., Oke (1987) and Incropera and DeWitt (1996)). For the case sketched in Fig. 3 showing one infinitely long wall adjacent to a street, the canopy and sky view factors for a ground-level position in the street are given by:

$$\Psi_{canopy} = (1 - \cos\beta)/2 \quad \text{and} \tag{7a}$$

$$\Psi_{sky} = (1 + \cos\beta)/2 \,, \tag{7b}$$

where β is equal to $\tan^{-1}(H/X)$, H is the wall height, and X is the shortest perpendicular distance between the wall and the point of interest. Urban areas, however, are not typically characterized by simple geometry. Therefore the collection of fish-eye images allows the complexity of urban geometry to be easily taken into account when computing sky view factor (see Methods section).

Sky View Factor Applications.

Sky view factors are often used in canopy radiation budget models in order to simplify the calculations. In ray tracing techniques, trajectories for a very large number of rays originating from the point of interest are computed, and their interception by surfaces along with reflections and re-emissions are calculated. The use of sky view factors, although introducting approximations, allows one to characterize the radiation transport between surfaces in an integrated fashion and therefore the number of computations are reduced dramatically. For example, Johnson et al. (1991) derived a formula for the net longwave energy at surface A_i for a street canyon with uniformly heated street and walls:

$$L_{net_i} = L_{down} - L_{up} = (L_{sky} + L_{walls} + L_{reflected})_{down} - L_{up} \tag{8}$$

$$= \Psi_{sky}\varepsilon_i\sigma T_{sky}^4 + \varepsilon_i \sum_{\substack{j=1 \\ i \neq j}}^{N} \Psi_{ji}\, \varepsilon_j\sigma T_j^4 + \varepsilon_i\sigma \sum_{\substack{k=1 \\ k \neq i}}^{N} \sum_{\substack{j=1 \\ j \neq k}}^{N} \Psi_{ki}\, (1-\varepsilon_k)\Psi_{jk}\, \varepsilon_j T_j^4 - \varepsilon_i\sigma T_i^4 ,$$

where ε_i is the emissivity of surface i and σ is the Stefan-Boltzman constant. Shortwave radiation balance equations have been derived as well using view factors (e.g., Ca et al., 1999; Masson, 2000).

In addition, it has been found that sky view factor correlates well with bulk properties of the urban environment. For example, Nunez et al. (2001) related the downward longwave radiative flux measurements to Ψ_{sky} with the following best-fit equation

$$L_{down} = -93.1\, \Psi_{sky} + 390.5 . \tag{9}$$

Furthermore, Oke (1987, p 293) found that for calm winds the heat island intensity itself is a function of the sky view factor:

$$\Delta T_{u\text{-}r(max)} = 15.27 - 13.88\, \Psi_{sky} , \tag{10}$$

where $\Delta T_{u\text{-}r(max)}$ is the maximum nightly temperature difference between the urban and rural areas. This relationship can be explained by noting that urban heat island development at night is partly due to decreased longwave radiation loss in the city. The urban area cools off more slowly at night compared to the surrounding rural terrain because the longwave cooling is decreased due

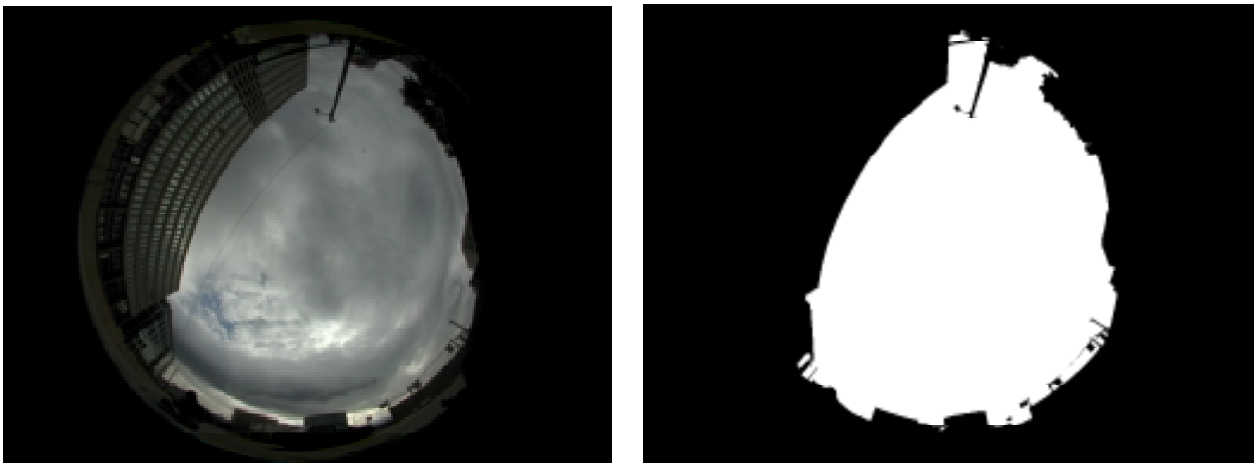

Figure 4. Fish-eye image before and after being processed.

to reduced sky view factor in the city, i.e., longwave loss from the surface to space is reduced and a fraction of the longwave emitted by the warm walls is towards the ground.

Method For Determining Sky View Factor.

In the Salt Lake City study, a digital camera (Nikon CoolPix 950) with a fish-eye hemispheric lens (Nikon FC-E8) is used to take the *in situ* observations. The Nikon lens used has a field of view (FOV) of 189° (Grimmond et al. 2001). The images are converted from color to black (ground, buildings, and vegetation) and white (sky) by altering the brightness and contrast of each image using Jasc Software's Paint Shop Pro (Fig. 4). When scattered clouds appear in an image, particularly near the horizon, the clouds often appear as dark as buildings or vegetation in the image, which makes it more difficult to set appropriate brightness values to discriminate terrain and sky. The black and white images are saved in portable greymap (jpg) format. To determine the total Ψ_{sky} at each site the equation of Johnson and Watson (1984) is used:

$$\varphi_{sky} = \frac{1}{2\pi}\sin\frac{\pi}{2n}\sum_{i=1}^{n}\sin\left[\frac{\pi(2i-1)}{2n}\right]\alpha_i \qquad (11)$$

where n is the total number of annuli, i is the annuls number and α_i is the total angular extent of sky visible in each annulus. This is done using the Grimmond et al. (2001) FORTRAN program (svf.exe). This program automatically detects the resolution of the image taken, and allows the user to specify the FOV to be analyzed; i.e. corrections to 180° were included at this stage.

Measurements.

Table 1 gives the approximate location where each photo was taken and the computed sky view factor. The table includes a photo identification number, the computed Ψ_{sky} value, a location in universal transverse mercator (UTM) coordinates (NAD 83, ZONE 12), the camera height at which the photo was taken, and the filename of the graphic image. The fish-eye images are found

in Appendix A at reduced size. It should be noted that the position determined using a hand-held GPS was found to be inadequate and therefore locations were determined from field notes and a building footprint map. We estimate the accuracy of the reported locations to be within a few meters with respect to distance from building walls. In regard to the camera height, the camera was mounted on a small tripod with legs of about 15 cm. "Ground" signifies that the camera tripod was placed on the street or sidewalk. Photos with id number 105 and greater were taken at rooftop level at the location of the LANL wind sensor sites. These photos are not included in the figures or calculated statistics provided below.

Figure 5 shows the approximate location where each street-level photo was taken relative to the building footprints. The majority of photos were taken around the release site near 400 S and State Streets and in the most built-up areas along Main St. and 100 S. Figure 6 shows the general location of where the photos were taken on a Salt Lake City street map. Figure 7 depicts the sky view factor computed at each location. A red color means that Ψ_{sky} is large indicating there are few canopy obstructions, while a purple color means that Ψ_{sky} is small meaning that the canopy is dense and the sky is obscured. Clearly the sky view factor is smallest in narrow alleyways and in regions close to tall buildings. One should also note that many trees were planted along open streets and contributed to reduced sky view factor (see images in Appendix A). The Ψ_{sky} observed in downtown Salt Lake City ranged from 0.33 to 0.90 with an average of 0.70. A histogram of the computed sky view factor (Fig. 8) shows that the majority of values fall in the 0.5 to 0.9 range. It is difficult to precisely compare the computed Ψ_{sky} with other cities because of the dependency on the spatial distribution of camera location positions (i.e., middle of the street vs. sidewalk, alleyways vs. main thoroughfares, parks vs. parking lots vs. built-up areas). However, given the size and structure of the buildings of the study area, the sky view factors are of the magnitude expected. Oke (1981) in a compilation of urban heat island studies, reported sky view factors for downtown sites ranging from 0.25 to 0.84. Barring et al. (1985) in a study of Malmo, Sweden measured sky view factors in the center of the city ranging from 0.5 to 1.0, while values in the suburbs were lower. Grimmond et al. (2001) in a study of a small U.S city, Bloomington, Indiana, using the same method employed here, calculated values in the range 0.39 to 0.99 (mean 0.83). A histogram of building heights in the study area shows greater than 90% of the buildings being between 3.5 and 87.5 m and a mode of 10.5-17.5 m (Fig. 9). The plan area density λ_p was computed as 0.33, while the frontal area density λ_p varied from 0.25 to 0.36 depending on wind direction. This information might prove useful when comparing our sky view factor measurements to other cities.

Data Files.

This report, a spreadsheet, and fish-eye images are available on the URBAN web site hosted by Lawrence Livermore National Laboratory. The report is in pdf format and the spreadsheet is available in MS Excel or text formats. The fish-eye images are in jpeg format with image size of approximately 14 x 11 inches at a resolution of 72 dpi, and are from 120 - 150 K in size. The image filenames are given in Table 1 in this report. All images are presented in Appendix A at reduced size. The spreadsheets contain information on each photo, including computed sky view factor, utm location, height above ground, and a written description of the site location. There are also columns of data that were produced during the sky view factor calculations. See Grimmond et al. (2001) for more details on the significance of these variables.

Table 1: Salt Lake City Fish-Eye Photos and Sky View Factor

id	SVF	UTMX(m)	UTMY(m)	Height	Input File
1	0.814	425135	4513206	ground	Dscn0861.jpg
2	0.816	425177	4513203	ground	Dscn0862.jpg
4	0.841	425193	4513198	1.67 m	Dscn0864.jpg
5	0.872	425234	4513182	ground	Dscn0865.jpg
6	0.883	425259	4513182	ground	Dscn0866.jpg
7	0.835	425265	4513215	ground	Dscn0867.jpg
8	0.901	425287	4513232	ground	Dscn0868.jpg
10	0.770	425287	4513262	ground	Dscn0870.jpg
11	0.792	425259	4513291	ground	Dscn0871.jpg
12	0.598	425224	4513276	ground	Dscn0872.jpg
13	0.757	425217	4513287	ground	Dscn0873.jpg
14	0.698	425188	4513267	ground	Dscn0874.jpg
15	0.553	425177	4513310	ground	Dscn0875.jpg
16	0.637	425177	4513346	ground	Dscn0876.jpg
17	0.837	425129	4513345	ground	Dscn0877.jpg
18	0.825	425115	4513334	ground	Dscn0878.jpg
19	0.825	425113	4513300	ground	Dscn0879.jpg
20	0.639	425102	4513270	ground	Dscn0880.jpg
21	0.773	425064	4513268	ground	Dscn0881.jpg
22	0.802	425060	4513239	ground	Dscn0882.jpg
23	0.630	425002	4513213	ground	Dscn0883.jpg
24	0.477	425025	4513190	ground	Dscn0884.jpg
25	0.747	425051	4513211	on ledge at 1 m	Dscn0885.jpg
26	0.711	425079	4513209	on ledge at 1 m	Dscn0886.jpg
27	0.685	425118	4513218	ground	Dscn0887.jpg
28	0.706	425172	4513219	ground	Dscn0888.jpg
29	0.349	425189	4513230	ground	Dscn0889.jpg

Table 1: Salt Lake City Fish-Eye Photos and Sky View Factor

id	SVF	UTMX(m)	UTMY(m)	Height	Input File
30	0.337	425187	4513256	ground	Dscn0890.jpg
35	0.750	425171	4512709	ground	Dscn0895.jpg
36	0.627	425158	4512721	ground	Dscn0896.jpg
37	0.550	425161	4512792	ground	Dscn0897.jpg
38	0.525	425161	4512772	ground	Dscn0898.jpg
39	0.523	425161	4512767	ground	Dscn0899.jpg
40	0.587	425152	4512746	ground	Dscn0900.jpg
41	0.822	425174	4512811	ground	Dscn0901.jpg
42	0.811	425204	4512812	ground	Dscn0902.jpg
43	0.807	425260	4512814	ground	Dscn0903.jpg
44	0.832	425247	4512777	on ledge at 2/3 m	Dscn0904.jpg
45	0.565	425286	4512755	ground	Dscn0905.jpg
46	0.762	425314	4512740	ground	Dscn0906.jpg
47	0.321	425342	4512767	ground	Dscn0907.jpg
48	0.852	425341	4512701	ground	Dscn0908.jpg
49	0.697	425357	4512730	ground	Dscn0909.jpg
50	0.794	425286	4512693	ground	Dscn0910.jpg
51	0.851	425251	4512649	ground	Dscn0911.jpg
52	0.816	425282	4512649	ground	Dscn0912.jpg
53	0.880	425256	4512582	ground	Dscn0913.jpg
54	0.888	425252	4512552	ground	Dscn0914.jpg
55	0.836	425206	4512552	ground	Dscn0915.jpg
56	0.822	425168	4512552	ground	Dscn0916.jpg
58	0.836	425131	4512554	ground	Dscn0918.jpg
59	0.835	425131	4512551	ground	Dscn0919.jpg
60	0.873	425108	4512553	ground	Dscn0920.jpg
61	0.876	425076	4512553	ground	Dscn0921.jpg

Table 1: Salt Lake City Fish-Eye Photos and Sky View Factor

id	SVF	UTMX(m)	UTMY(m)	Height	Input File
62	0.537	425077	4512502	ground	Dscn0922.jpg
63	0.506	425120	4512502	ground	Dscn0923.jpg
64	0.799	424790	4512590	ground	Dscn0924.jpg
65	0.689	424789	4512615	ground	Dscn0925.jpg
66	0.670	424790	4512636	ground	Dscn0926.jpg
67	0.671	424789	4512657	ground	Dscn0927.jpg
68	0.713	424789	4512691	ground	Dscn0928.jpg
69	0.736	424790	4512724	ground	Dscn0929.jpg
70	0.627	424789	4512755	ground	Dscn0930.jpg
71	0.666	424789	4512787	ground	Dscn0931.jpg
72	0.625	424792	4512832	ground	Dscn0932.jpg
73	0.447	424793	4512886	on stone pedestal	Dscn0933.jpg
74	0.578	424795	4512944	ground	Dscn0934.jpg
75	0.584	424796	4512993	ground	Dscn0935.jpg
76	0.598	424796	4513032	ground	Dscn0936.jpg
77	0.580	424794	4513072	ground	Dscn0937.jpg
78	0.585	424792	4513117	ground	Dscn0938.jpg
79	0.646	424792	4513165	ground	Dscn0939.jpg
80	0.692	424791	4513214	ground	Dscn0940.jpg
81	0.783	424792	4513271	ground	Dscn0941.jpg
82	0.713	424793	4513315	ground	Dscn0942.jpg
83	0.532	424795	4513369	ground	Dscn0943.jpg
84	0.581	424794	4513418	ground	Dscn0944.jpg
86	0.650	424792	4513554	ground	Dscn0946.jpg
88	0.629	424746	4513536	ground	Dscn0948.jpg
90	0.705	424677	4513533	ground	Dscn0950.jpg
91	0.784	424604	4513535	ground	Dscn0951.jpg

Table 1: Salt Lake City Fish-Eye Photos and Sky View Factor

id	SVF	UTMX(m)	UTMY(m)	Height	Input File
92	0.866	424577	4513536	ground	Dscn0952.jpg
93	0.888	424550	4513515	ground	Dscn0953.jpg
94	0.866	424548	4513457	ground	Dscn0954.jpg
95	0.854	424554	4513368	ground	Dscn0955.jpg
96	0.840	424553	4513319	ground	Dscn0956.jpg
98	0.654	424618	4513294	ground	Dscn0958.jpg
99	0.682	424695	4513292	raised media ~0.5 m	Dscn0959.jpg
100	0.088	424726	4513322	raised media ~0.5 m	Dscn0960.jpg
101	0.790	424820	4513293	ground	Dscn0961.jpg
102	0.680	424904	4513288	ground	Dscn0962.jpg
103	0.715	424950	4513290	raised media ~0.5 m	Dscn0963.jpg
104	0.718	425013	4513291	ground	Dscn0964.jpg
images at LANL met. station locations; camera placed at roof level					
828	0.987	425105	4513235	Federal Bldg	828svf_fedbldg.jpg
838	0.835	425200	4512678	Parking Lot	838svf_parkinglot.jpg
839	0.838	425200	4512678	Parking Lot	839svf_parkinglot#2.jpg
847	0.993	425212	4512628	10th Fl. City Centre	847svf_citycent10fl.jpg
848	0.981	425212	4512628	10th Fl. City Centre	848svf_citycent10fl.jpg
859	0.929	425180	4512665	4th Fl. NW City Centre	859svf_4flcitycentNW.jpg
860	0.840	425232	4512597	4th Fl. SE City Centre	860svf_4flcitycentSE.jpg
861	0.995	425212	4512743	Heber Wells	861svf_HeberWells.jpg
862	0.996	425212	4512628	10th Fl. City Centre	862svf_Citycenter.jpg
863	0.988	425105	4513235	Federal Bldg.	863svf_FedBldg.jpg
864	0.995	425212	4512743	Heber Wells	864svf_Wells.jpg

Figure 5. The approximate locations of where fish-eye photographs were taken in downtown Salt Lake City relative to building footprints. The numbers correspond to the photo id as given in Table 1.

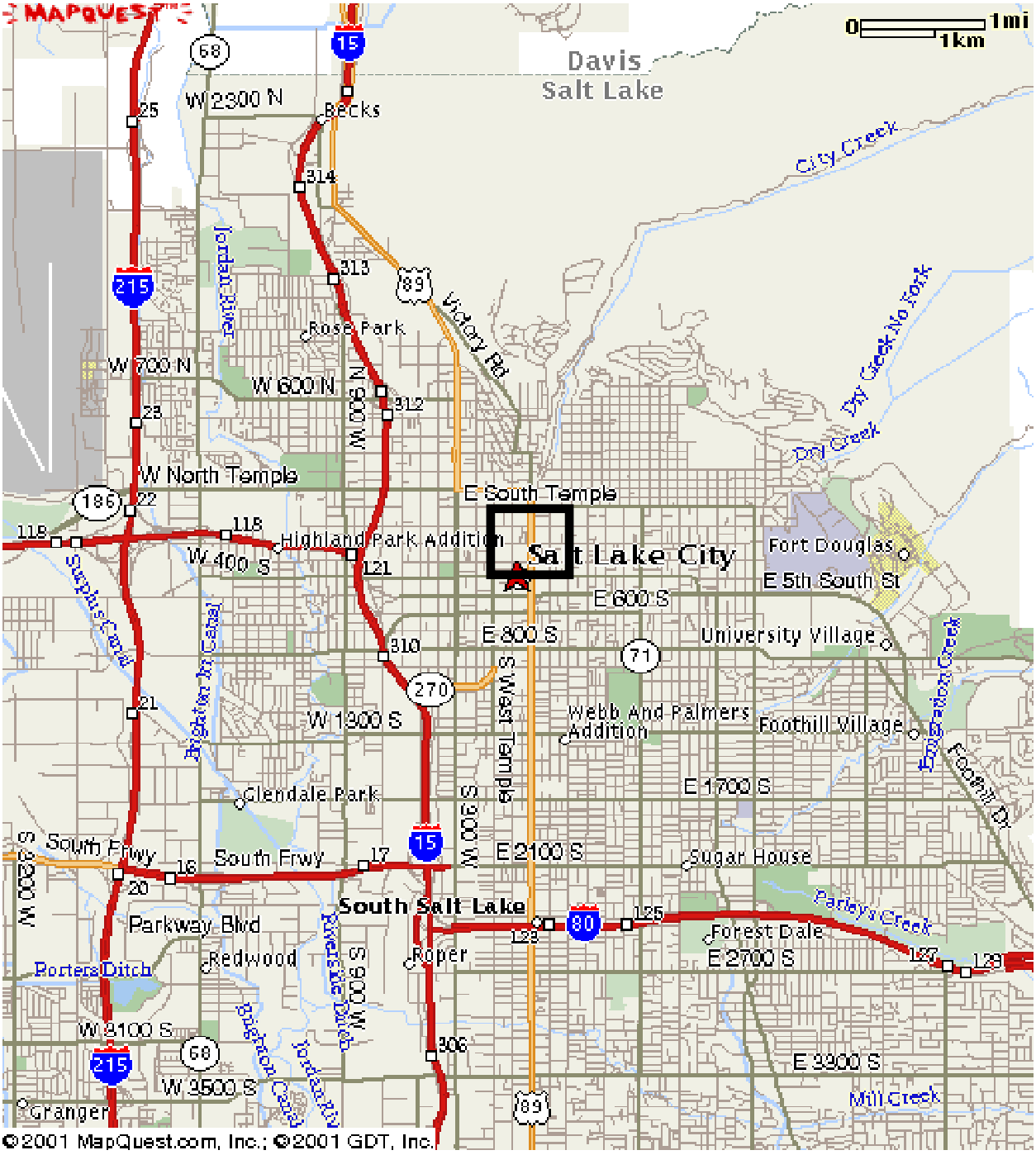

Figure 6. Street map of Salt Lake City showing the downtown location (denoted by the black box) where the fish-eyefish-eye photos were taken.

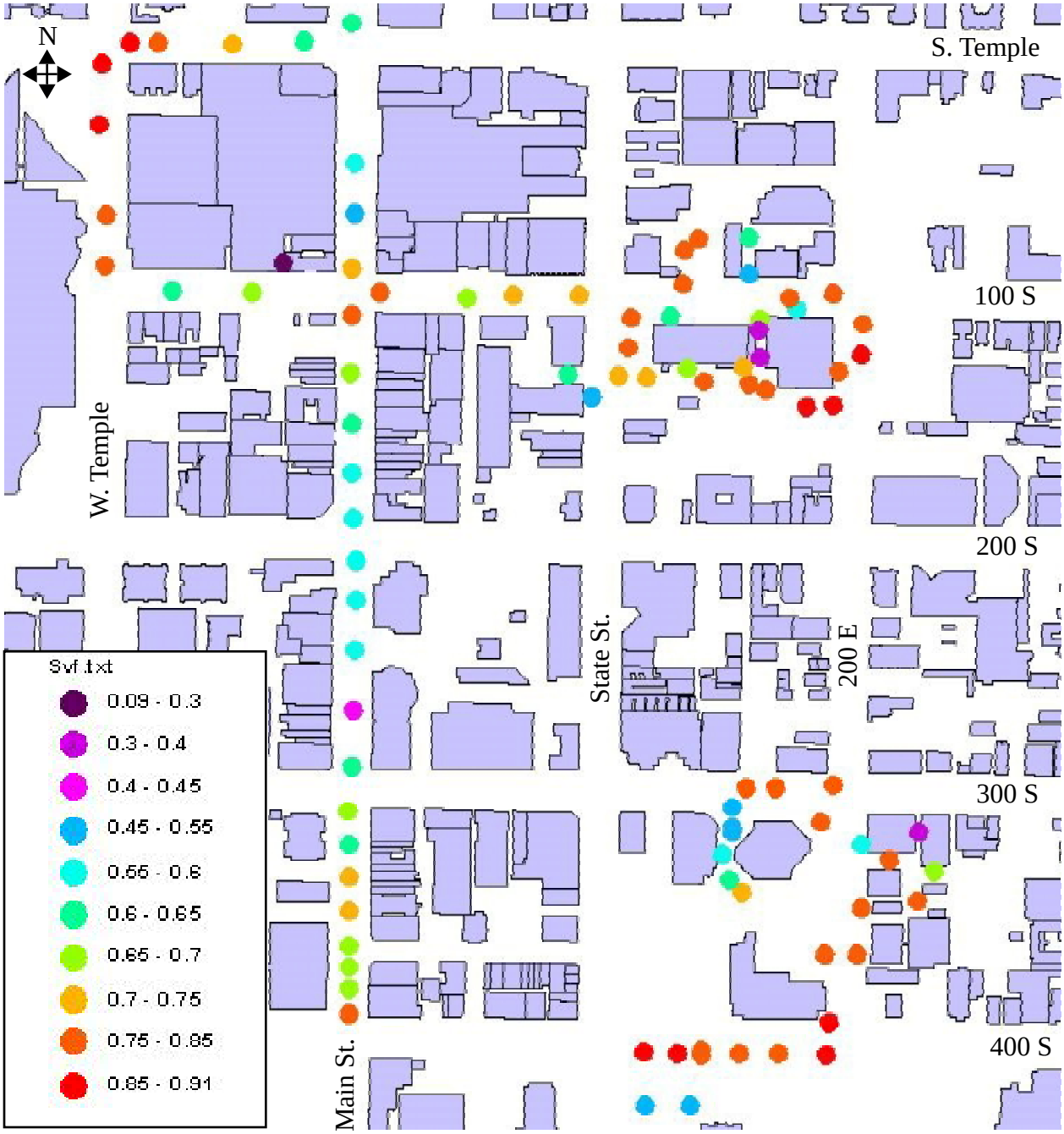

Figure 7. The computed sky view factor overlaid onto downtown Salt Lake City building footprint map. Photos taken Oct. 22, 2000.

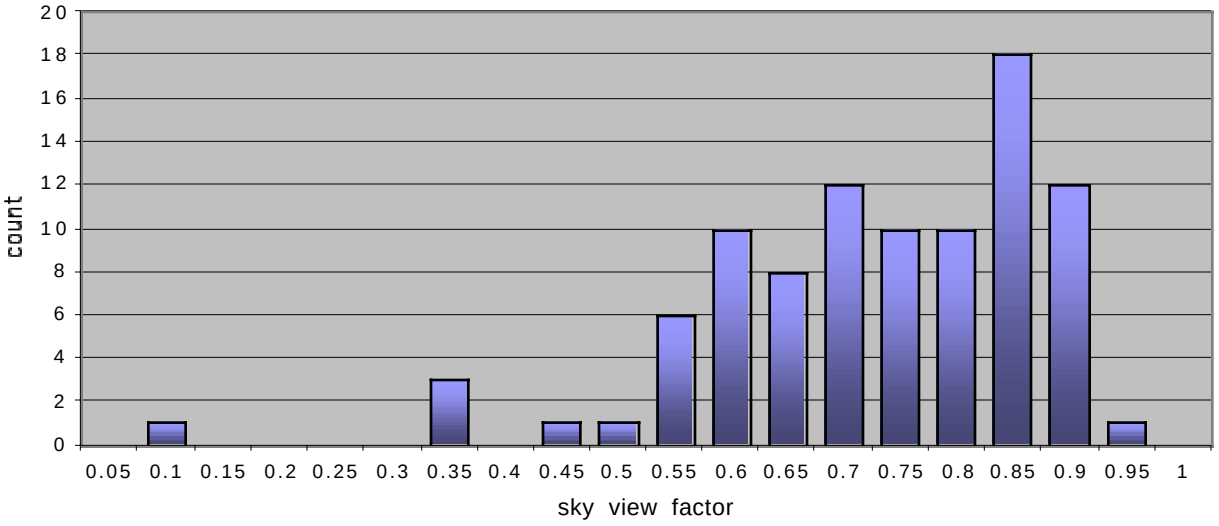

Figure 8. A histogram of the computed sky view factor for street-level positions in downtown Salt Lake City. Photos taken Oct. 22, 2000 and do not include rooftop images.

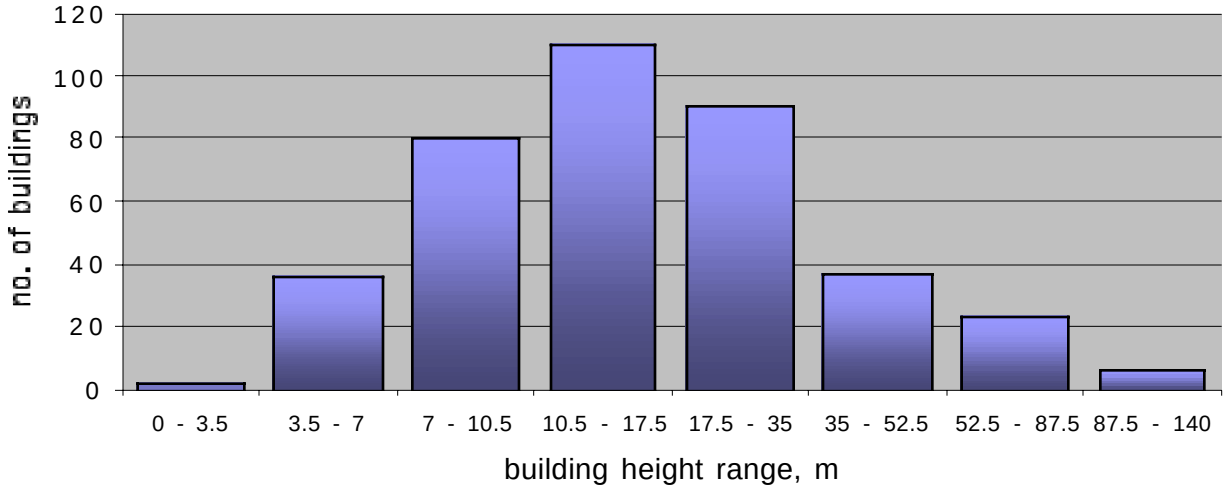

Figure 9. A histogram of the building heights for the study area in downtown Salt Lake City.

For more information regarding access to the URBAN web site contact:

Dr. Ron Calhoun
LLNL, L-103, NARAC Facility
Livermore, CA 94550
(925) 422-1841, e-mail: calhoun7@llnl.gov

The data described in this report can also be obtained directly from the authors of this report.

Acknowledgements.

Special thanks go to Shane Hubbard (Indiana University) for converting the sky view factor images to pgm format, to Steve Linger (Los Alamos National Laboratory) for converting photograph location coordinates from latitude/longitude to universal transverse mercator (utm), to Tim McPherson and Steve Linger (Los Alamos National Laboratory) for help with producing maps using ArcView GIS software, to Steve Burian (University of Arkansas) for providing the building height histogram and plan/frontal area calculations, and to Ingegärd Eliasson for her suggestions to improve the report.

References.

Barring et al. (1985) Canyon geometry, street temperatures, and urban heat island in Malmo, Sweden, Journ. Climatology, 5, 433-444.

Ca, V., T. Asaeda, and Y. Ashie (1999) Development of a numerical model for the evaluation of the urban thermal environment, J. Wind Eng. Ind. Aerodyn., 81,181-196.

Grimmond, C.S.B., S.K. Potter, H.N. Zutter, and C. Souch (2001) Rapid methods to estimate sky view factors applied to urban areas, Int. Journ. Climatology. (in press).

Incropera, F. and D. DeWitt (1996) Fundamentals of Heat and Mass Transfer, John Wiley and Sons, New York, NY.

Johnson, T., T. Oke, T. Lyons, D. Steyn, I. Watson, and J. Voogt (1991) Simulation of surface urban heat islands under “ideal” conditions at night, Part 1: Theory and tests against field data, Bound.-Layer Meteor., 56, 275-294.

Johnson, G.T. and I.D. Watson (1984) The determination of view factors in urban canyons, Journ. Clim. and Appl. Meteor., 2, 329-335.

Masson, V. (2000) A physically-based scheme for the urban energy budget in atmospheric models, Bound.-Layer Meteor., 94, 357-397.

Nunez, M., I. Eliasson, and J. Lindgren (2001) Spatial variations of incoming longwave radiation in Goteberg, Sweden, Theor. Appl. Climatol., 67, 181-192.

Oke, T. (1987) Boundary Layer Climates, Routledge, London.

Oke, T. (1981) Canyon geometry and the nocturnal urban heat island: comparison of scale model and field observations, Journ. Climatology, 1, 237-254.

Watson, I. and G. Johnson (1987) Graphical estimation of sky view-factors in urban environments, Journ. Climatology, 7, 193-197.

Appendix A. Fish-eye Images

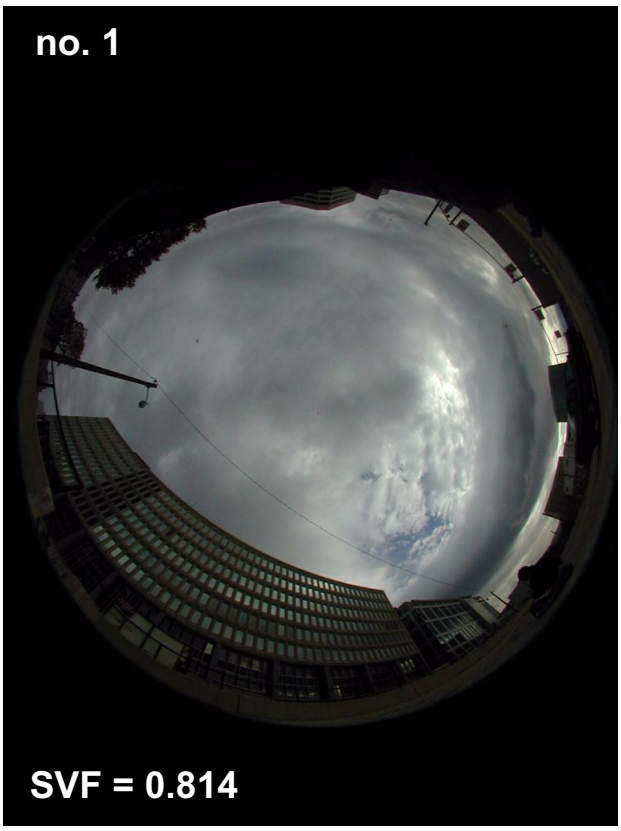
no. 1
SVF = 0.814


no. 2
SVF = 0.816


no. 4
SVF = 0.841

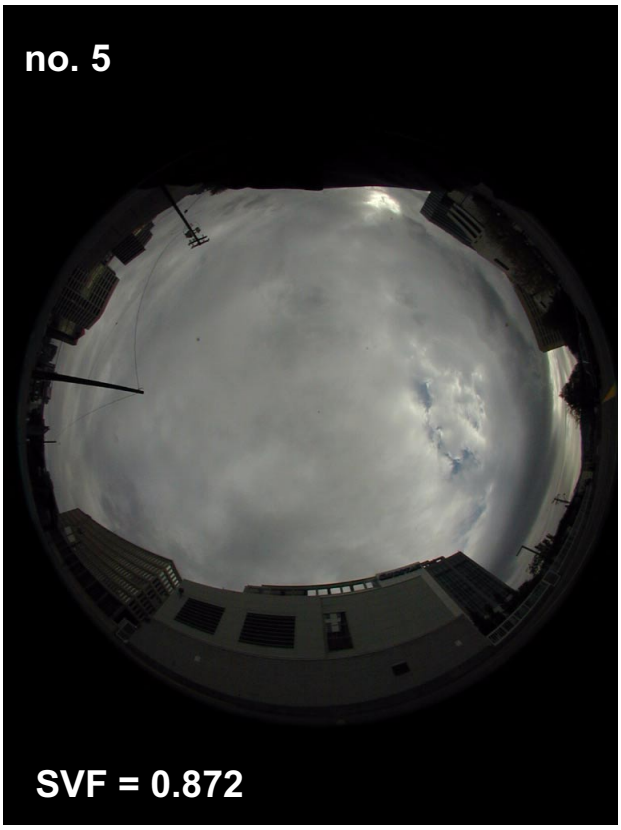
no. 5
SVF = 0.872


no. 6
SVF = 0.883


no. 7
SVF = 0.835

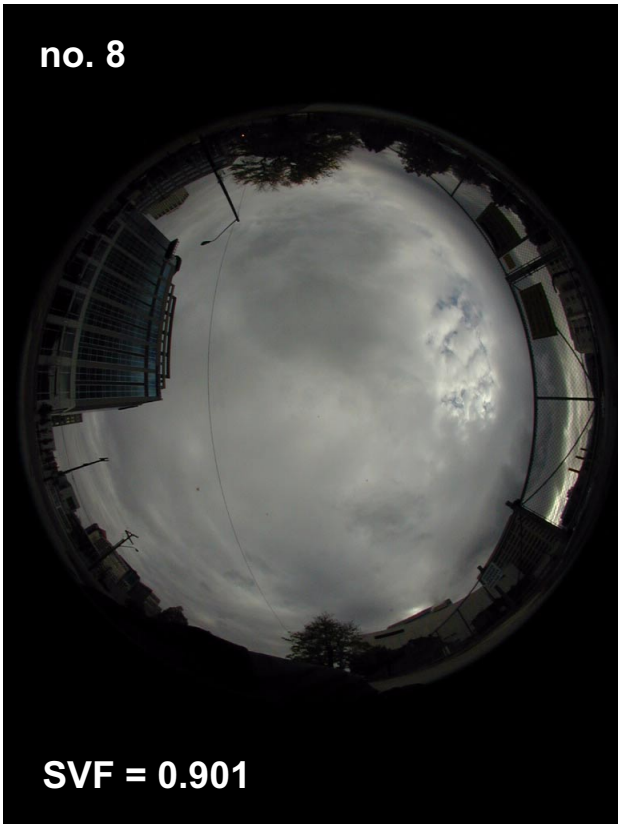
no. 8
SVF = 0.901


no. 10
SVF = 0.770


no. 11
SVF = 0.792


no. 12
SVF = 0.598


no. 13
SVF = 0.757


no. 14
SVF = 0.698


no. 15
SVF = 0.553


no. 16
SVF = 0.637


no. 17
SVF = 0.837


no. 18
SVF = 0.825


no. 19
SVF = 0.825


no. 20
SVF = 0.639


no. 21
SVF = 0.773


no. 22
SVF = 0.802


no. 23
SVF = 0.630


no. 24
SVF = 0.477


no. 25
SVF = 0.747


no. 26
SVF = 0.711

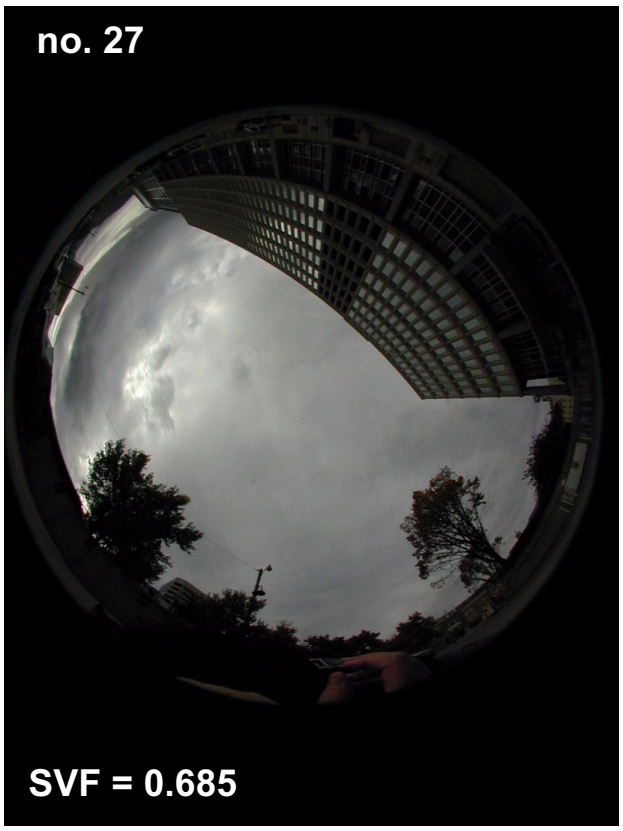
no. 27
SVF = 0.685


no. 28
SVF = 0.706


no. 29
SVF = 0.349


no. 30
SVF = 0.337


no. 35
SVF = 0.750


no. 36
SVF = 0.627


no. 37
SVF = 0.550

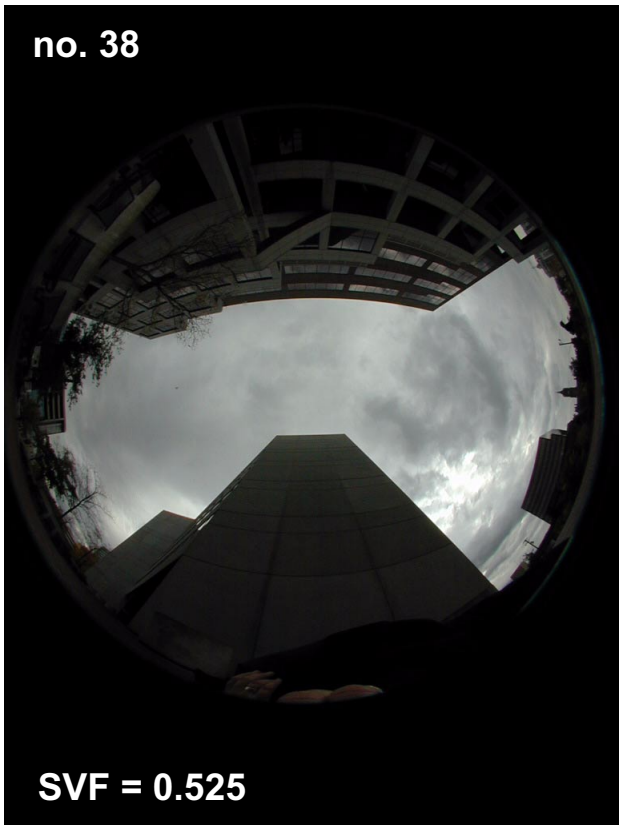
no. 38
SVF = 0.525


no. 39
SVF = 0.523


no. 40
SVF = 0.587


no. 41
SVF = 0.822


no. 42
Antique Time
CLOCKS · FURNITURE · MUSIC BOXES · REPAIRS · RESTORATION
SVF = 0.811


no. 43
ANTIQUES & CHINA MATCHING
SVF = 0.807


no. 44
SVF = 0.832


no. 45
SVF = 0.565


no. 46
SVF = 0.762


no. 47
SVF = 0.321


no. 48
SVF = 0.852

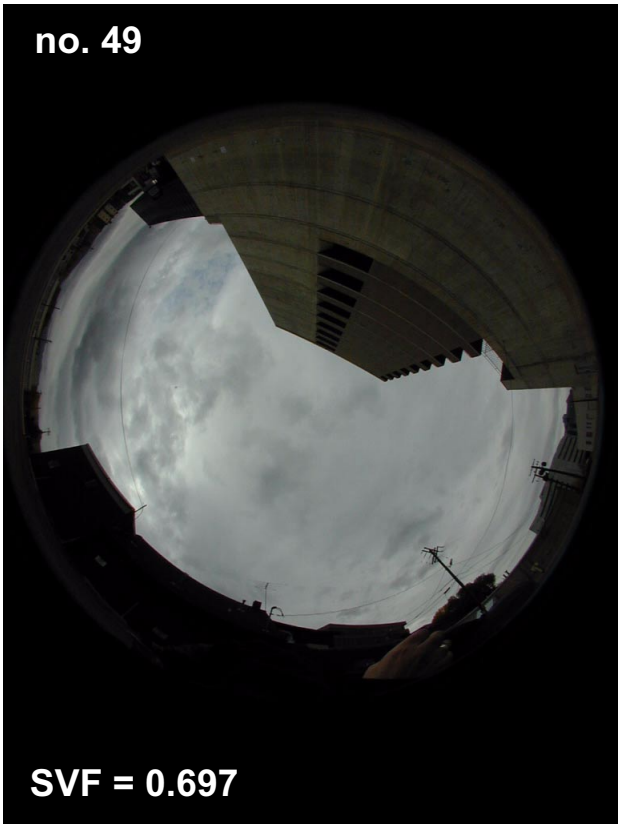
no. 49
SVF = 0.697


no. 50
SVF = 0.794

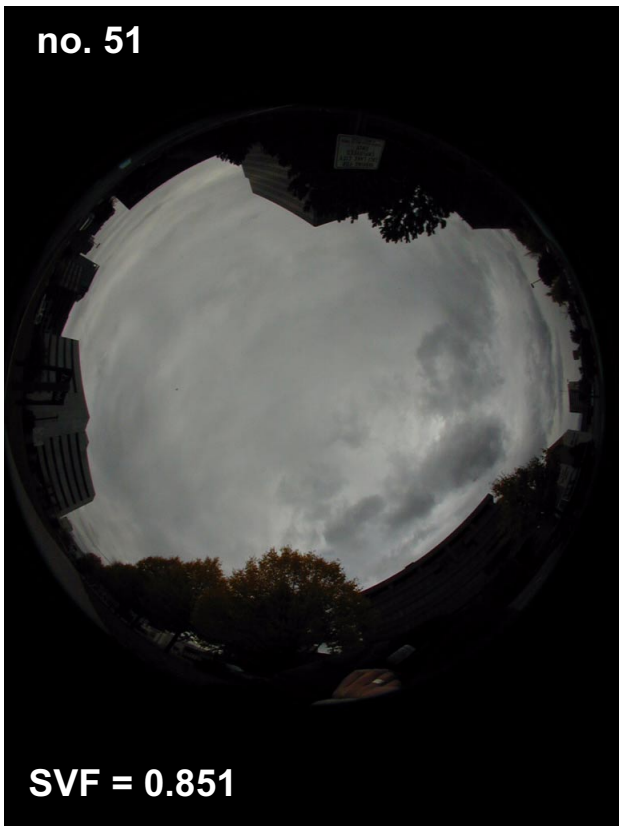
no. 51
SVF = 0.851


no. 52
SVF = 0.816


no. 53
SVF = 0.880


no. 54
SVF = 0.888


no. 55
SVF = 0.836


no. 56
SVF = 0.822


no. 58
SVF = 0.836


no. 59
SVF = 0.835


no. 60
SVF = 0.873


no. 61
SVF = 0.876


no. 62
SVF = 0.537


no. 63
SVF = 0.506


no. 64
SVF = 0.799


no. 65
SVF = 0.689


no. 66
SVF = 0.670


no. 67
SVF = 0.671


no. 68
SVF = 0.713


no. 69
SVF = 0.736


no. 70
SVF = 0.627


no. 71
SVF = 0.666


no. 72
SVF = 0.625

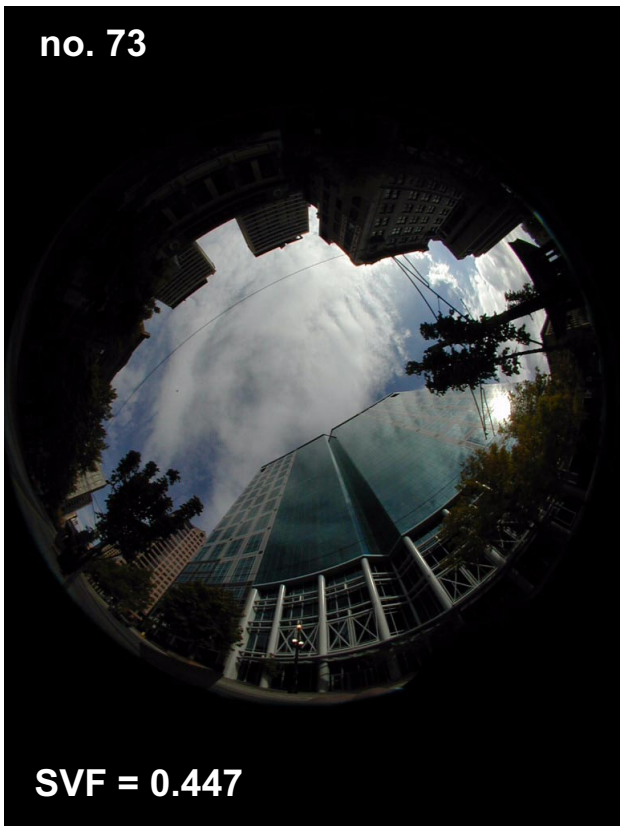
no. 73
SVF = 0.447


no. 74
SVF = 0.578


no. 75
SVF = 0.584


no. 76
SVF = 0.598


no. 77
SVF = 0.580


no. 78
SVF = 0.585


no. 79
SVF = 0.646


no. 80
SVF = 0.692


no. 81
SVF = 0.783


no. 82
SVF = 0.713


no. 83
SVF = 0.532


no. 84
SVF = 0.581


no. 86
SVF = 0.650


no. 88
SVF = 0.629


no. 90
SVF = 0.705


no. 91
SVF = 0.784


no. 92
SVF = 0.866


no. 93
SVF = 0.888

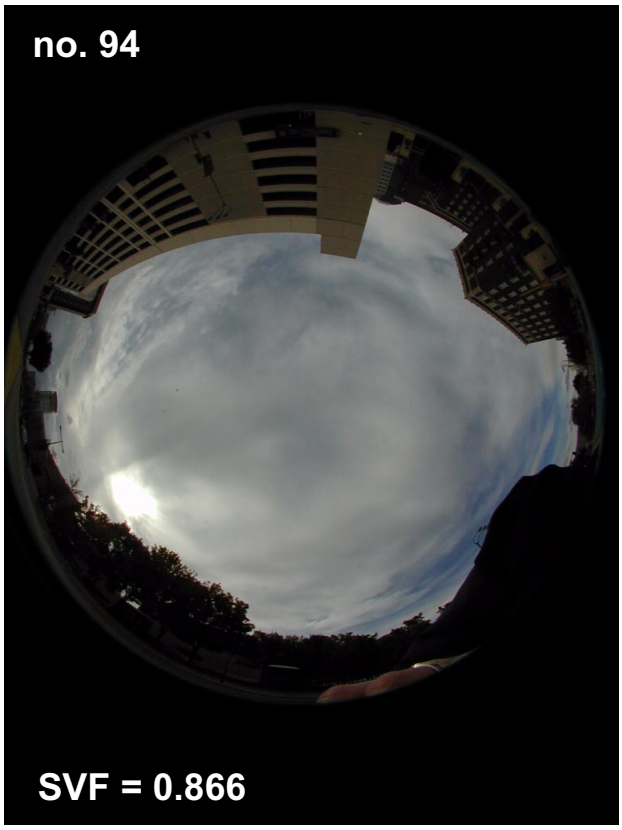
no. 94
SVF = 0.866


no. 95
SVF = 0.854


no. 96
SVF = 0.840


no. 98
SVF = 0.654


no. 99
SVF = 0.682

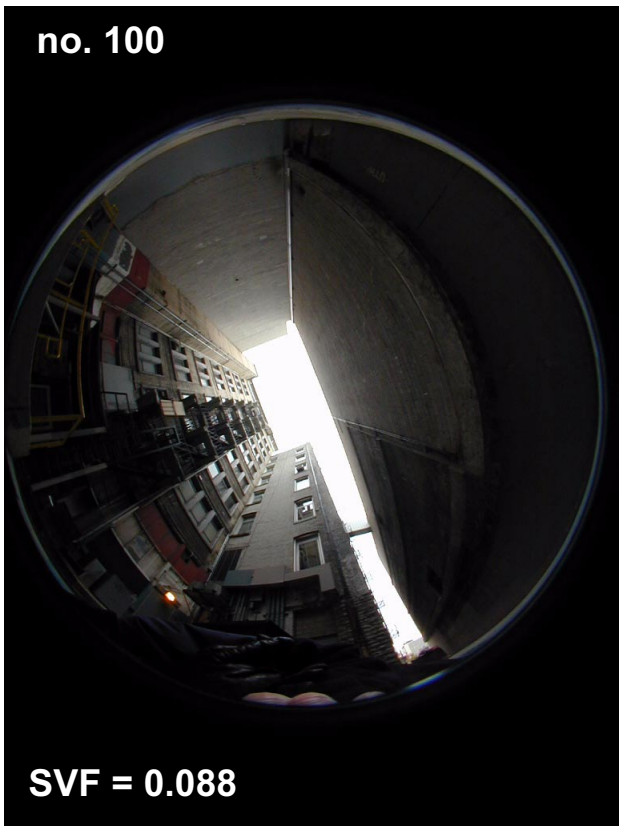
no. 100
SVF = 0.088


no. 101
SVF = 0.790


no. 102
THE ZCMI CENTER
SVF = 0.680


no. 103
THE ZCMI CENTER
SVF = 0.715


no. 104
SVF = 0.718

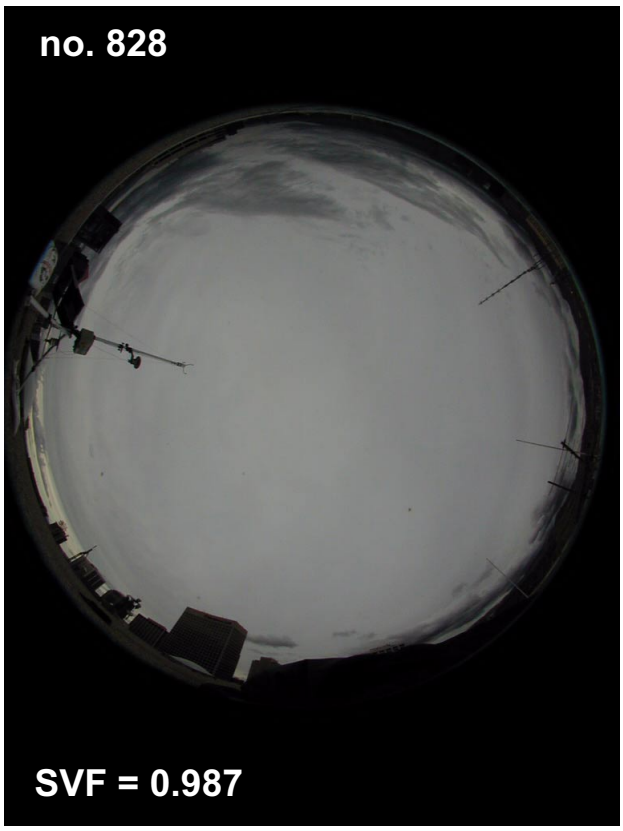
no. 828
SVF = 0.987

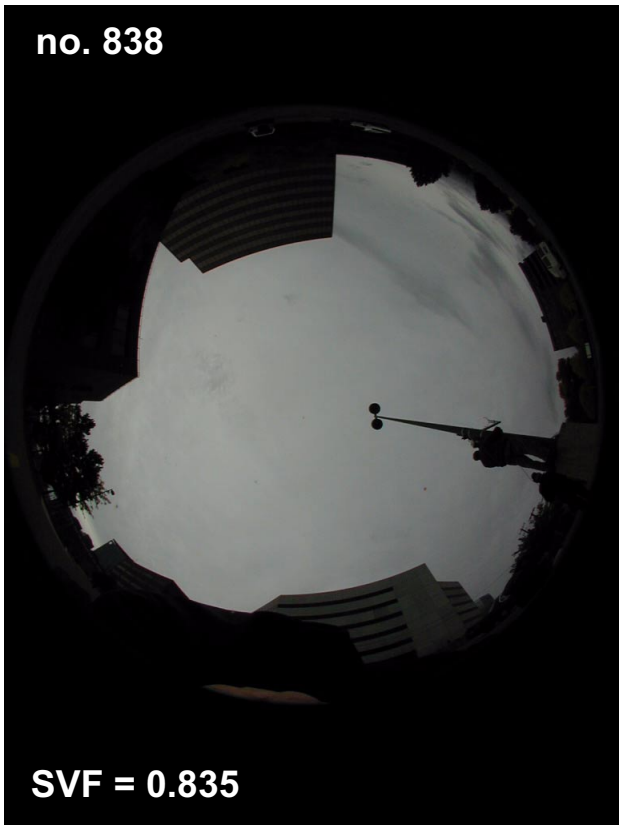
no. 838
SVF = 0.835

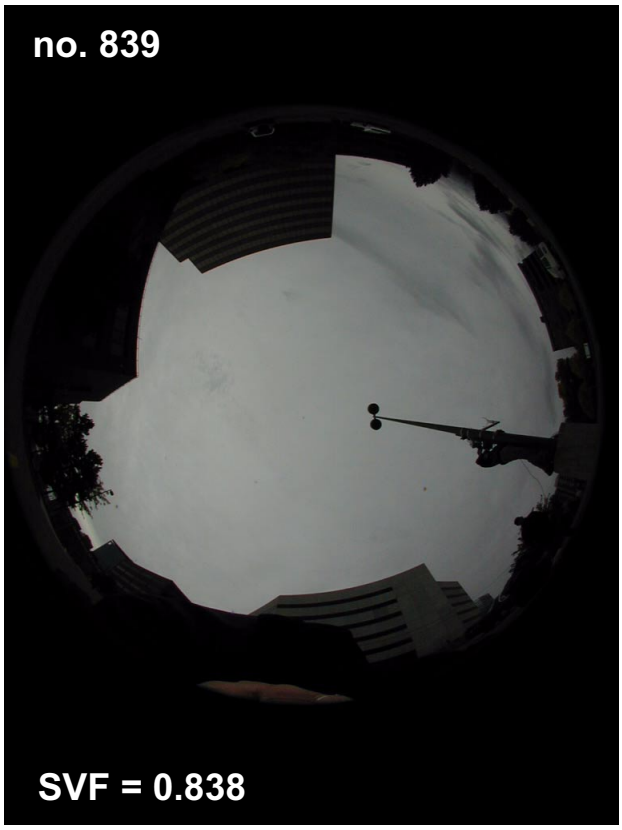
no. 839
SVF = 0.838

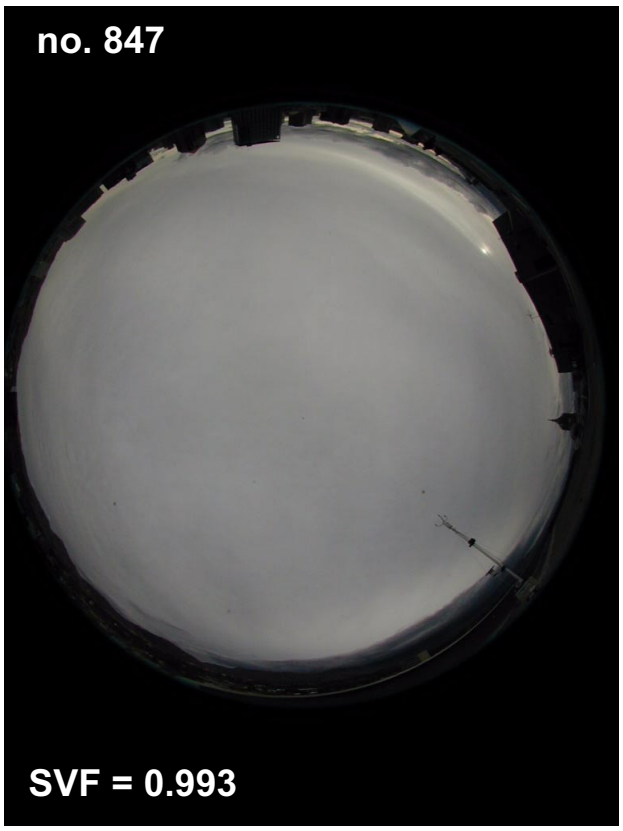
no. 847
SVF = 0.993

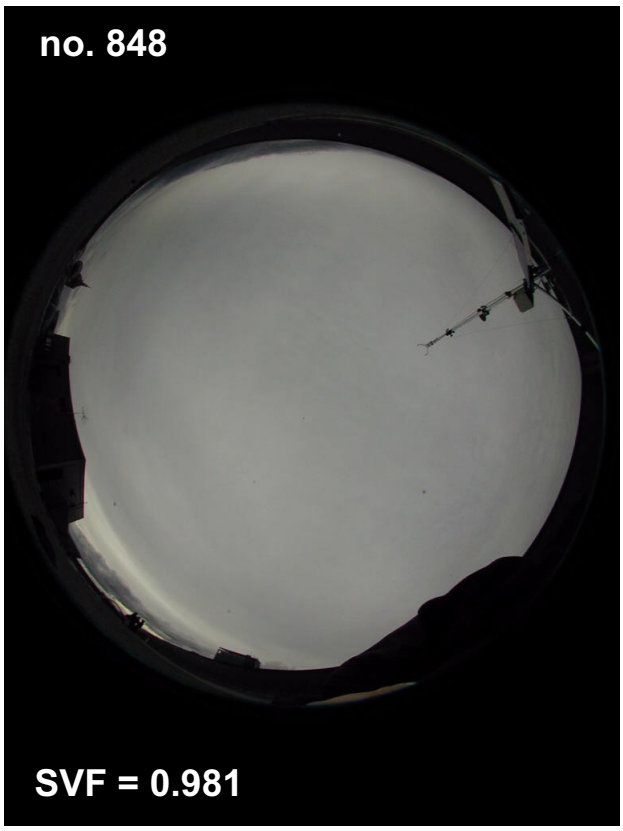
no. 848
SVF = 0.981

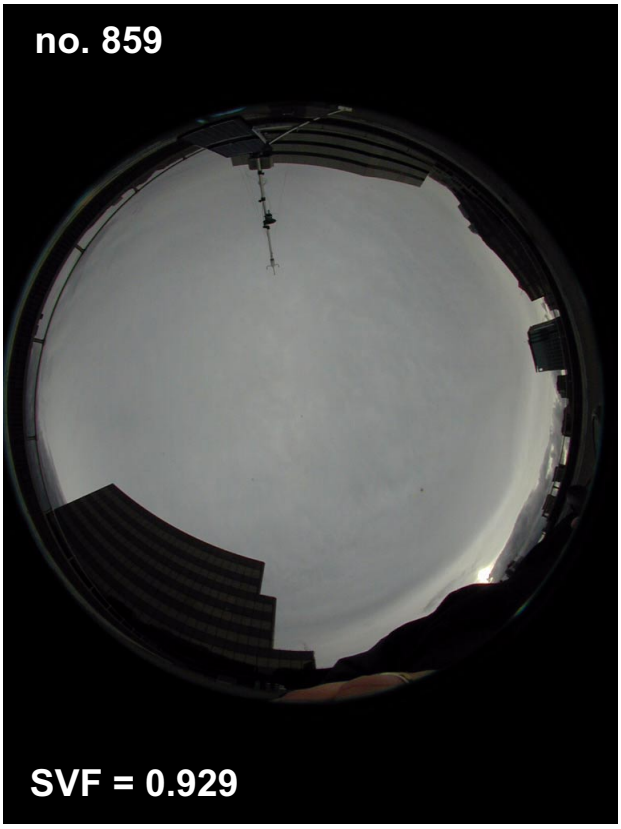
no. 859
SVF = 0.929


no. 860
SVF = 0.840

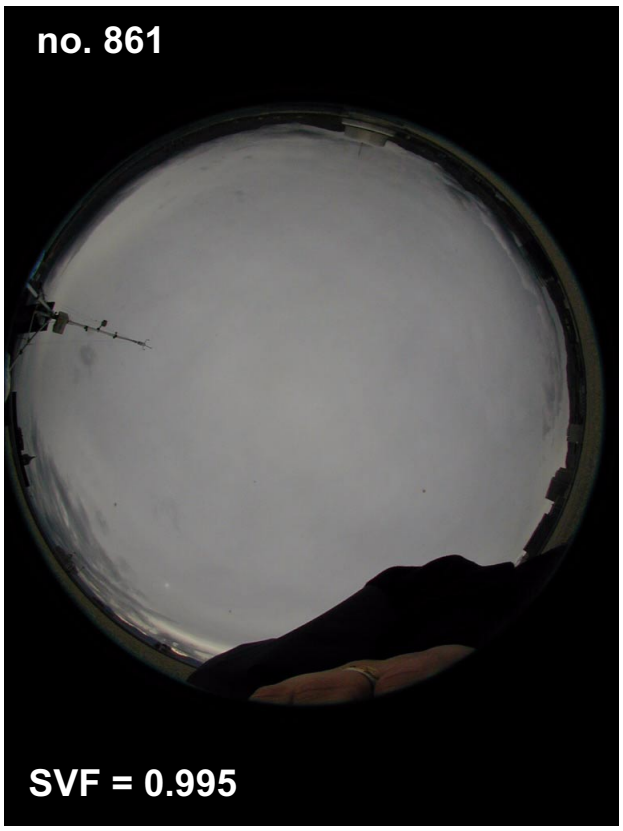
no. 861
SVF = 0.995

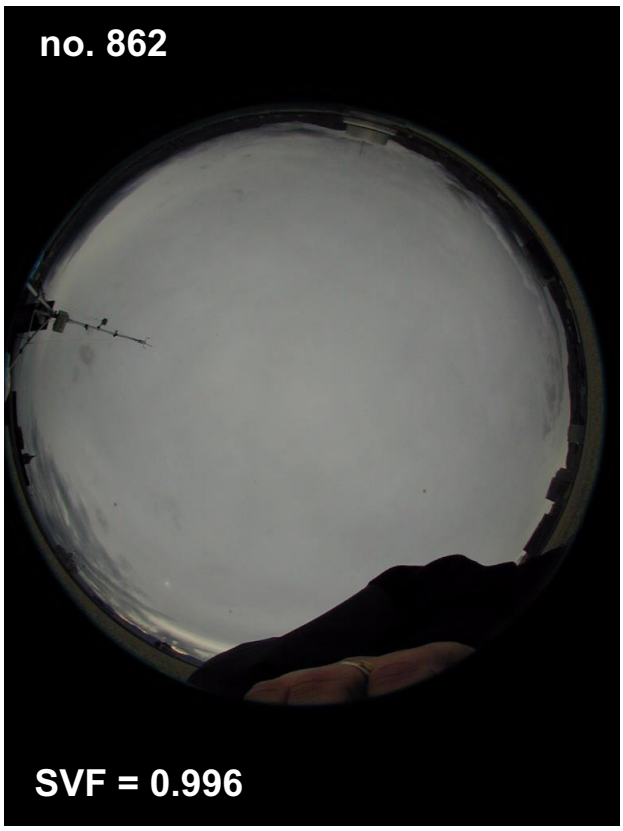
no. 862
SVF = 0.996

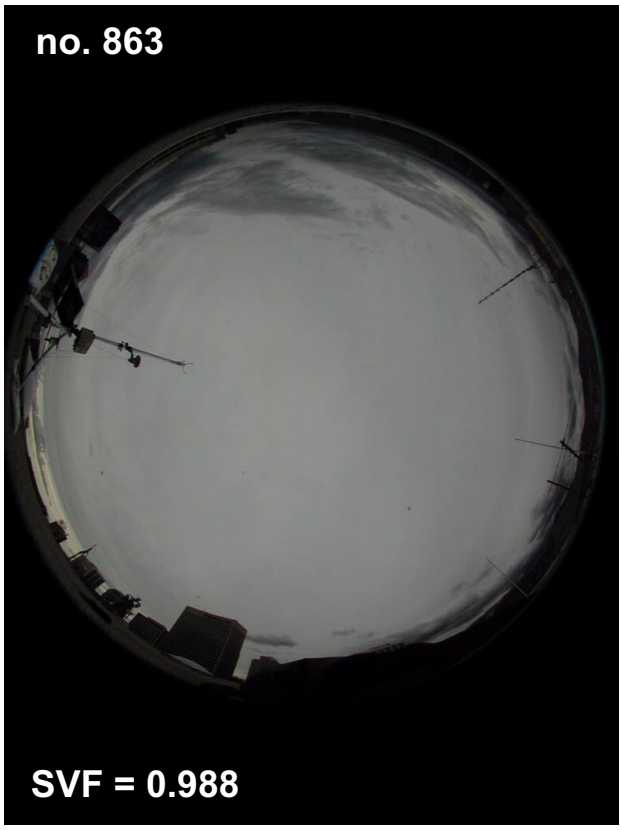
no. 863
SVF = 0.988


no. 864
SVF = 0.995